ORIGINAL ARTICLE

Chitosan-sodium alginate-polyethylene glycol-crocin nanocomposite treatment inhibits esophageal cancer KYSE-150 cell growth via inducing apoptotic cell death

Anxi Hu [a], Abdullah A. Alarfaj [b], Abdurahman Hajinur Hirad [b],
Vishnu Priya Veeraraghavan [c], Krishna Mohan Surapaneni [d],
Samer Hasan Hussein-Al-Ali [f], Nandakumar Natarajan [e], Poorni Kaliyappan Elayappan [g,*]

[a] Department of Thoracic Surgery, Zhengzhou Central Hospital affiliated to Zhengzhou University, Zhengzhou City, Henan Province 450001, China
[b] Department of Botany and Microbiology, College of Science, King Saud University, P.O. Box 2455, Riyadh 11451, Saudi Arabia
[c] Centre of Molecular Medicine and Diagnostics (COMManD), Department of Biochemistry, Saveetha Dental College & Hospitals, Saveetha Institute of Medical and Technical Sciences, Saveetha University, Chennai 600 077, India
[d] Department of Biochemistry, Panimalar Medical College Hospital & Research Institute, Varadharajapuram, Poonamallee, Chennai 600 123, India
[e] Department of Surgery, Immunogenetics and Transplantation Laboratory, University of California San Francisco, San Francisco, CA, USA
[f] Faculty of Pharmacy, Isra University, Amman 11622, Jordan
[g] Department of Biochemistry, Vivekanantha College of Arts and Sciences for Women (Autonomous), Elayampalayam, Tiruchengode, Namakkal, Tamil Nadu 637205, India

Abstract *Background:* Esophageal cancer is a sixth most cause of cancer-associated mortalities worldwide with increased global prevalence in each year. It has a poor prognosis with 5-year survival rate are less than 10%.
  Objective: The present study was focused to fabricate the chitosan-sodium alginate-polyethylene glycol-crocin nanocomposites (CSP-Cr-NCs) and evaluate its *in vitro* anticancer potential against the esophageal cancer KYSE-150 cells.

* Corresponding author.
  E-mail address: Biochempoorni@gmail.com (P.K. Elayappan).
Peer review under responsibility of King Saud University.

Production and hosting by Elsevier

Methodology: The fabricated CSP-Cr-NCs were characterized using different techniques such as UV–visible spectroscopy, photoluminescence assay, DLS analysis, XRD, SEM and EDX analyses. The antimicrobial study was conducted by well diffusion technique against the *S. pneumoniae, K. pneumoniae, E. coli, S. aureus,* and *C. albicans.* The viability of CSP-Cr-NCs treated KYSE-150 and Het-1A cells were assessed by the MTT assay. The ROS production, MMP level, and apoptotic cell death in the CSP-Cr-NCs administered cells were assessed by using different fluorescent staining techniques. The cell migration of CSP-Cr-NCs treated KYSE-150 cells were assessed by wound scratch assay. The levels of TBARS, GSH, and SOD activity in the CSP-Cr-NCs treated KYSE-150 cells were assessed by kits.

Results: The outcomes from the different characterization analyses witnessed the formation of CSP-Cr-NCs with the 100–210 nm size, tetragonal and agglomerated morphological appearances. The CSP-Cr-NCs effectively repressed the microbial growth. The CSP-Cr-NCs treated KYSE-150 cells were demonstrated the decreased cell viability and IC50 was found at 2.5 μg, furthermore it did not affected the normal Het-1A cells. The formulated CSP-Cr-NCs treatment at 2.5 and 5 μg improved the ROS production, and decreased the MMP status in the KYSE-150 cells. The elevated incidences of apoptotic cells death was found in the CSP-Cr-NCs treated KYSE-150 cells. The CSP-Cr-NCs also inhibited the migration of KYSE-150 cells. The increased TBARS content and decreased GSH and SOD activity was also found in the CSP-Cr-NCs treated KYSE-150 cells.

Conclusion: Our findings proved that the formulated CSP-Cr-NCs treatment effectively inhibited the esophageal cancer KYSE-150 cell growth via increasing ROS production and apoptotic cell death. Therefore, it could be a promising anticancer candidate in the future for the esophageal cancer treatment.

1. Introduction

Esophageal cancer is a most common malignant tumor and it ranks 6th in terms of mortality worldwide with poor survival rate (Bray et al., 2018). In spite of clinical advancements in the area of oncology, esophageal cancer still remains as one of the major reasons of cancer-related deaths. The overall 5-year survival rate of esophageal cancer patients is reported to less than 20% (O'Sullivan et al., 2018). The esophageal cancer still remains as a challenging disease to treat due to its aggressive nature and poor response to therapies. The delayed diagnosis, metastasis, and lack of effective treatment strategies are the critical factors of the poor survival rate of esophageal cancer of patients (Kuo et al., 2016). Apoptosis is a programmed cell death and important physiological event participate in the exclusion of injured cells. The dysregulation of pro-apoptotic and anti-apoptotic genes were reported in several tumors (Cheng et al., 2018). The increasing of ROS level in tumor cells either by stimulation of direct ROS generation or depletion of antioxidant mechanisms in tumor cells could facilitate to the cell death. Many previous reports suggested that the activation of over ROS accumulation in tumor cells is the main underlying mode of action of conventional therapies (Kim et al., 2019).

Several chemotherapeutic drugs elevate the ROS production and can change the redox homeostasis of tumor cells. The doxorubicin, cisplatin, cyclophosphamide, topoisomercisplatin, camptothecins, and arsenic agents are some of the effective drugs that can increase the ROS accumulation in tumor cells but these drugs often reported with serious adverse effects (Yang et al., 2018; Zhu et al., 2016). In recent times, the therapeutic strategies available for the cancer treatment is highly life threatening and trigger organs dysfunction that in turn worsen the life expectancy of patients, also to be costly (Hugtenburg et al., 2019).

The failure of radiotherapy and chemotherapy results in tumor recurrence and poor prognosis primarily due to the adverse effects and incomplete efficacy, for instance, chemotherapeutic drugs target both tumor and normal cells leading to toxic effects (Wang et al., 2018). Therefore, the need for the discovery of stable, effective, and safer drug candidates are highly warranted.

Nanomedicine has unlocked a novel approaches to overwhelm several difficulties in cancer treatment, however not yet been implemented in clinical settings as projected. Nanomedicines are broadly investigated systems for huge number of therapeutic candidates (Bor et al., 2019). Polymeric nanocomposites are extensively encouraged as a biomaterials due to their promising characteristics like easy formulation and design, considerable biocompatibility, a wide-range of structures and other peculiar characteristics (El-Say and El-Sawy, 2017). The biodegradable polymeric nanocomposites are the talented candidates for the development of anticancer modalities with the properties of sustained release. The nanostructures can considerably increase the therapeutic effects of chemotherapeutic drugs. The tumor-targeted nanomedicines are believed to further advance the systems to evade cytotoxicity to normal cells and increase therapeutic effects (Swain et al., 2016). The drug design and development uses several nanotechnologies to improve the cancer treatment strategies (Afzal et al., 2021). The nanotechnology receives greater attention in developing the novel drug carrier and delivery system. Nano-carriers will transport drug molecules to targeted sites and are predicted to kill the tumor cells without affecting normal cells (Huang et al., 2020).

Chitosan is a deacetylated chitin, a well known biopolymer that presents naturally as the fungal cell wall component, exoskeleton of insects, and the crustacean shells. It is already reported that chitin demonstrated several pharmacological benefits like less toxic nature, biocompatibility and degradability (Chadchawan and Pichyangkura, 2015). Chitosan is extensively utilized as a carrier of polymeric nanoformulations for drug delivery (Munawar et al., 2017). The polyethylene glycol (PEG)-based coatings on the nanomedicines and its applications was well-reported (Hadjesfandiari and Parambath, 2018; Suk et al., 2016). The PEG coating enables extended circulating period by evading opsonization, consequently, the applications of PEG-coated nano-drug systems were highlighted in several previous reports (Mishra et al., 2016). The use of PEG polymer is believed to offer a improved drug-loading and extended circulation period. These properties is due to the occurrence of surface PEG molecules. It was also reported that nanocomposites with PEG polymer demonstrates improved drug delivery (Wilkosz et al., 2018).

Crocin is a bioactive carotenoid compound extensively found in the saffron. It was reported that crocin offered several pharmacological activities like renoprotective (Hosseinzadeh et al., 2008), anti-oxidant (Yaribeygi et al., 2018), anti-depressant (Alavizadeh and Hosseinzadeh, 2014) and anti-inflammatory (Zhu et al., 2019) effects. Additionally, several previous literatures reported that crocin effectively inhibited the growth of several tumors like colorectal cancer (Amerizadeh et al., 2018), cervical cancer (Mollaei et al., 2017), retinoblastoma (Deng et al., 2019), and gastric cancer (Zhou et al., 2019). To enhance the therapeutic effects and targeted activity of crocin, the present study focused to fabricate the chitosan-sodium alginate-polyethylene glycol-crocin nanocomposites (CSP-Cr-NCs) and evaluate its *in vitro* anticancer property against the esophageal cancer KYSE-150 cells.

2. Materials and methods

2.1. Chemicals

Crocin, polyethylene glycol, chitosan, sodium alginate, Dulbecco's Modified Eagle's Medium (DMEM), 3-(4,5-dimethyl thiazoyl-2-yl)-2,5-diphenyltetrazolium bromide (MTT), and other reagents were acquired from Sigma-Aldrich, USA. The assay kits for biochemical assays were purchased from the Thermofisher Scientific, USA.

2.2. Synthesis of CSP-Cr-NCs

The CSP-Cr-NCs were formulated by using the previous methods explained by Qi et al. (2004) and Wathoni et al. (2019). For this, the crocin was dissolved in 20 mL of double distilled water and then suspended in the chitosan solution (0.1%, wt/vol) newly prepared in 1% acetate acid. The mixture was stirred constantly until the formation of reaction suspension. For reducing the nanoparticles, the reaction solution was ultra-sonicated and then the reaction solution that contains chitosan and crocin was added into the polymer solution, which is prepared using polyethylene glycol and sodium alginate for coating of the developed nanoparticles. The coating process was achieved by microvolume flow titration method. After the coating process, the final reaction solution was dehydrated by spray pyrolysis technique to collect the developed nanocomposite powder. The formulated CSP-Cr-NCs were utilized for different characterization techniques.

2.3. Characterization of fabricated CSP-Cr-NCs

The development of CSP-Cr-NCs in suspension was confirmed by using the UV–visible spectral study. The CSP-Cr-NCs development was witnessed with the help of UV–vis spectral study and the absorbance of reaction solution was determined at wavelength varied from 200 to 1000 nm.

The photoluminescence spectrum of the formulated CSP-Cr-NCs were measured by using the spectrofluorimeter (F-2500 FL Spectrophotometer, Hitachi).

The distribution and average size of the formulated CSP-Cr-NCs were investigated by dynamic light scattering (DLS) analysis.

The developed CSP-Cr-NCs were examined by using the X-ray diffractometer (XRD, Malvern Panalytical) using Cu-Kα radiation of wavelength λ = 0.1541 nm in a scan range of 2θ = 10–80∘.

The formulated CSP-Cr-NCs and its surface bound functional groups were examined by fourier transform-infra red (FT-IR) analysis. Briefly, the prepared CSP-Cr-NCs sample was assessed by using FT-IR machine (IR Prestige-21; Shimadzu, Kyoto, Japan). The polymeric nanocomposites were amalgamated with KBr and then pellets were molded with vacuum pressure at 60 kN within 15 min, and examined at 4000–500 cm^{-1}.

The size, morphology and compositional analysis of fabricated CSP-Cr-NCs were done using scanning electron microscope attached with energy dispersive X-ray (SEM with EDXA, Sirion) apparatus.

2.4. Antibacterial assay

The CSP-Cr-NCs were dispersed into 1 mL of sterile 5% DMSO and utilized as a stock. The well diffusion technique was executed to examine the antimicrobial property of CSP-Cr-NCs. The microbial strains were *S. pneumoniae*, *K. pneumoniae*, *E. coli*, *S. aureus*, and *C. albicans* were treated with different concentrations (40, 50, and 60 µg) of CSP-Cr-NCs. The amoxicillin (30 µg/disc) were utilized as a standard. After the 24 h of treatment, the inhibition zones were recorded.

2.5. Cell culture maintenance

The human esophageal cancer KYSE-150 cells and normal esophageal epithelial cells Het-1A were grown on a DMEM enriched with FBS (10%) and maintained on 5% CO_2 supplied incubator at 37 °C. After reaching 80% confluency, the grown cells were trypsinized, and utilized for further assays.

2.6. MTT cytotoxicity assay

The viability of CSP-Cr-NCs treated KYSE-150 and Het-1A cells were assessed by using MTT cytotoxicity assay. In brief, both cells were seeded onto the separate 96-wellplate added with DMEM at 5×10^3 cell density/well and kept for 24 h at 37 °C for the adhesion. Later, the growth media of cells were replenished and supplemented with diverse doses of fabricated CSP-Cr-NCs (5–100 µg) for 24 h at 37 °C. After the treatment period, 20 µl of MTT and 100 µl of DMEM was added to each well and further maintained for 4 h at 37 °C. Later, 100 µl of DMSO was added to every well to dissolve the formed formazan crystals. The viability of control and treated cells were measured by taking absorbance at 570 nm using microplate reader.

2.7. Acridine orange/Ethidium bromide (AO/EB) dual staining

The level of apoptotic cell death in CSP-Cr-NCs treated KYSE-150 cells were assessed by AO/EB staining. In brief, KYSE-150 cells were seeded on 24-wellplate at 5×10^5 cell population/well and incubated for 24 h at 37 °C. After that, cells were administered with CSP-Cr-NCs at the dose of 2.5 and 5 µg and incubated for 24 h at 37 °C. Later than treatment period, 100 µg/ml of AO/EB stain at 1:1 ratio were used to stain the treated cells for 5 min. The apoptotic cell death in treated cells were assessed by using fluorescence microscope.

2.8. Intracellular ROS production

The level of ROS production in control and CSP-Cr-NCs supplemented KYSE-150 cells were assessed by using DCFH-DA staining. Briefly, KYSE-150 cells were seeded on 24-wellplate with DMEM at 1×10^6 population and treated with 2.5 and 5 μg of CSP-Cr-NCs for 24 h at 37 °C. After the treatment period, the 10 μl of DCFH-DA dye was added to every well for 1 h to stain the cells. Finally, the ROS production level in control and treated cells were assessed using fluorescent microscope.

2.9. Assay of mitochondrial membrane potential (MMP)

The MMP level in control and CSP-Cr-NCs treated KYSE-150 cells were assessed by Rh-123 staining technique. For this, the KYSE-150 cells were loaded on 24-wellplate at 1×10^6 cell density/well and nurtured for 24 h at 37 °C. Afterward, cells were treated with 2.5 and 5 μg of CSP-Cr-NCs for 24 h at 37 °C. The 10 μg/ml of Rh-123 were utilized to stain the cells for 30 min and the intensity of fluorescence were observed using fluorescence microscope.

2.10. Propidium iodide (PI) staining

The incidences of apoptosis in control and CSP-Cr-NCs administered KYSE-150 cells were assessed by using PI staining technique. The KYSE-150 cells were loaded on the 24-wellplate with DMEM and incubated for 24 h at 37 °C. Afterward, the cells were supplemented with 2.5 and 5 μg of CSP-Cr-NCs for 24 h at 37 °C. After that, 5 μl of PI dye was added to each well for 20 min and finally fluorescent intensity was monitored using fluorescence microscope.

2.11. Cell viability assay

The level of cell adhesion and death in control and CSP-Cr-NCs treated KYSE-150 cells were assessed. For this, the KYSE-150 cells were placed on the gelatin-coated culture plate with DMEM for 24 h. Then the cells were treated with 2.5 and 5 μg of CSP-Cr-NCs and stand for 60 min at 37 °C. Later, cells were cleansed with saline solution then stained with trypan blue stain to identify the cell adhesion and death levels using light microscope.

2.12. Wound scratch assay

For wound scratch assay, the KYSE-150 cells were grown on 6-wellplate and after reaching 80% confluency, the wound scratch was made using the 200 μl micro tip in every well. The cells were cleansed using saline after the scratching to remove the detached cells. Then the undetached cells and treated with 2.5 and 5 μg of CSP-Cr-NCs and incubated for 24 h. Later, the cells were cleansed with saline for 30 sec and wound closure level was assessed and microphotographs were taken 0hr and 24 h using microscope.

2.13. Quantification of oxidant and antioxidant markers

The level of TBARS, antioxidant GSH and SOD in the lysates of control and 2.5 and 5 μg of CSP-Cr-NCs treated KYSE-150 cells were investigated by respective assay kits as per the protocols of manufacturer (Thermofisher Scientific, USA).

2.14. Statistical analysis

All values were assessed using GraphPad prism software and outcomes were depicted as mean ± SD of triplicate assays. The data examined by one-way ANOVA and Duncan's multiple range assay and significance was set at $p < 0.05$.

3. Results

3.1. Characterization of formulated CSP-Cr-NCs

The formation of CSP-Cr-NCs in the reaction solution was established by the UV–visible spectroscopic analysis and findings were illustrated in the Fig. 1(a). The absorbance were taken at different wavelengths (200–1000 nm). The maximum absorbance of formulated CSP-Cr-NCs were noted at 285 nm that evidences the development of CSP-Cr-NCs (Fig. 1a).

The developed CSP-Cr-NCs were investigated by photoluminescence study and result was showed in the Fig. 1(b). The fabricated CSP-Cr-NCs were demonstrated the excitations at 367 nm, 398 nm, 416 nm, 458 nm, 481 nm, 506 nm, respectively, which proves the occurence of CSP-Cr-NCs. The spectrum of photoluminescence analysis demonstrates the surface and structural defects and crystal modality of synthesized CSP-Cr-NCs. The free exciton recombination were found at the peaks 367 nm and 398 nm. The 416 nm, 458 nm, and 481 nm, peaks exhibits the blue-green and blue emissions due to the interstitial oxygen vacancies. The singly ionized oxygen vacancy in the developed CSP-Cr-NCs were confirmed by the green emission at 506 nm (Fig. 1b).

Fig. 1(c) demonstrated the distribution patterns and size ranges of synthesized CSP-Cr-NCs, which is studied by the DLS analysis. The outcomes of DLS study revealed the clear peaks, which confirms the narrowed distribution and size of CSP-Cr-NCs ranging from 100 to 210 nm.

The purity and crystalline nature of synthesized CSP-Cr-NCs were investigated by XRD analysis and data were depicted in the Fig. 2(a). The peaks of CSP-Cr-NCs were developed at (110), (002), (111), (−202), (020), (202), (−113), (−311), and (220) that witnesses the face-centered cubic structures. The XRD finding demonstrated the purity of the synthesized CSP-Cr-NCs (Fig. 2a).

The presence of functional groups in the formulated CSP-Cr-NCs were assessed by the FT-IR and data were depicted in the Fig. 2(b). The FT-IR spectral analysis of formulated CSP-Cr-NCs revealed a various peaks at several frequencies. The major peaks such as 3453 cm^{-1} exhibits the band due to O-H stretching. The 2884 cm^{-1} peak denotes the hydroxyl stretching. The 1638 cm^{-1} and 1097 cm^{-1} peaks denotes the C-H and C-O bending vibrations. The peaks at 946 cm^{-1} and 603 cm^{-1} exhibits the H-O bonds (Fig. 2b).

The size and appearance of synthesized CSP-Cr-NCs were examined by SEM and EDX analysis was executed to detect the compositions of CSP-Cr-NCs. The microphotographs of SEM indicates that the fabricated CSP-Cr-NCs exhibited tetragonal and agglomerated morphological appearances (Fig. 3a). The compositional analysis by EDX demonstrated
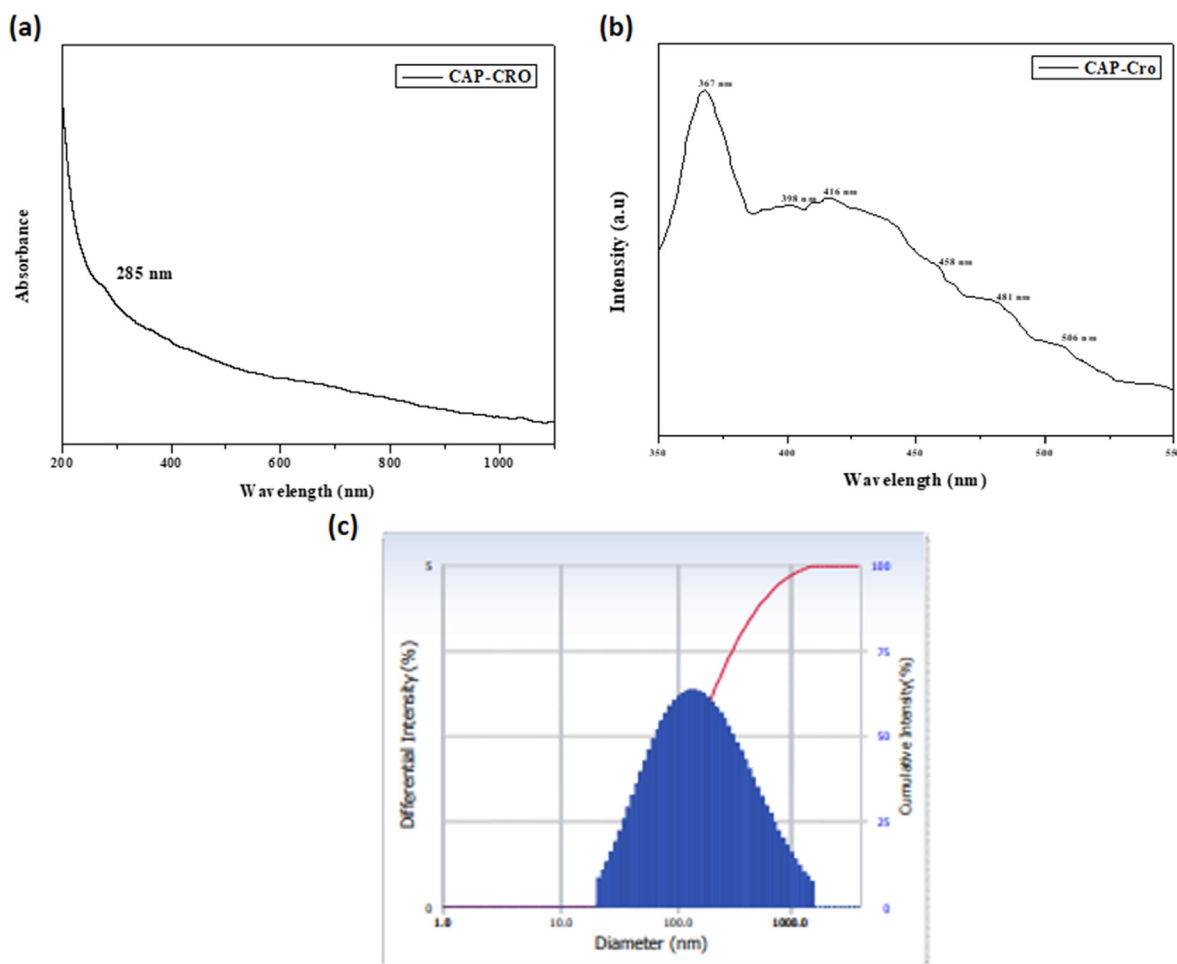
Fig. 1   UV–visible spectrum, photoluminescence, and DLS analysis of synthesized CSP-Cr-NCs. UV–Visible spectral analysis of formulated CSP-Cr-NCs showed the maximum peak at 285 nm **(a)**. Photoluminescence spectral analysis of synthesized CSP-Cr-NCs demonstrated the various excitation at 367 nm, 398 nm, 416 nm, and 458 nm, 481 nm, 506 nm, respectively **(b)**. The DLS study revealed the clear peak that confirms the narrowed distribution of formulated CSP-Cr-NCs and size ranging from 100 to 210 nm **(c)**.
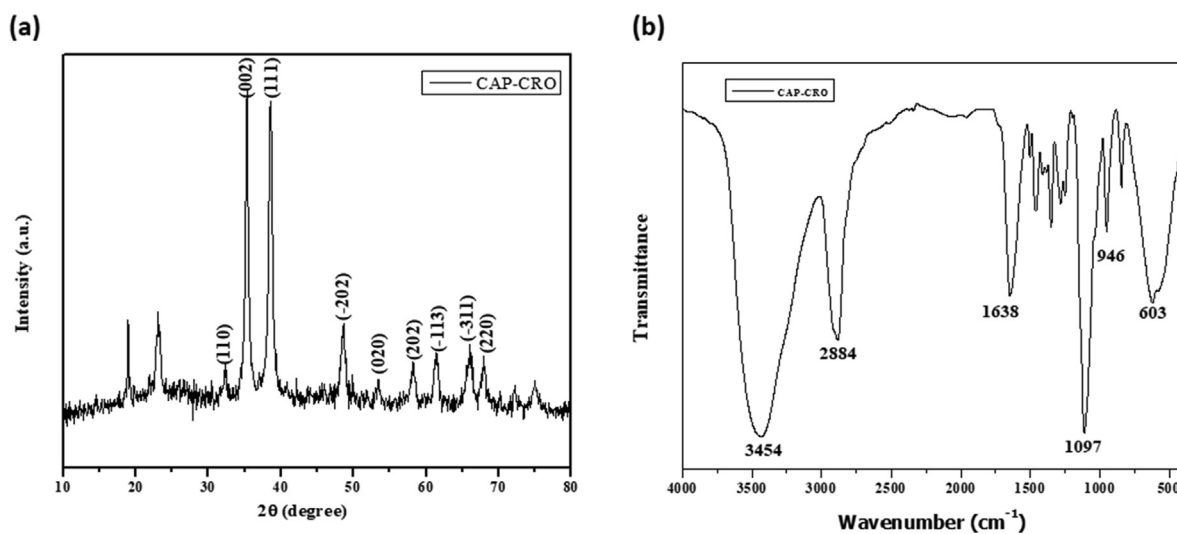
Fig. 2   XRD and FT-IR analysis of CSP-Cr-NCs. XRD analysis demonstrated the different peaks, which confirms the crystalline nature of fabricated CSP-Cr-NCs **(a)**. FT-IR spectrum of formulated CSP-Cr-NCs exhibited the presence of several stretching and bonding such as O-H, C-H, C-O, and H-O **(b)**.

that the fabricated CSP-Cr-NCs showed distinct peaks, which corresponds to the existence carbon, nitrogen, oxygen, and copper elements (Fig. 3b).

3.2. Antimicrobial activity of fabricated CSP-Cr-NCs

Fig. 4 demonstrates the antimicrobial activity of fabricated CSP-Cr-NCs against *S. pneumoniae, K. pneumoniae, E. coli, S. aureus,* and *C. albicans* strains, which was studied by the well diffusion technique. The findings clearly exhibited that the fabricated CSP-Cr-NCs effectively inhibited the growth of tested strains, which is evidenced by the increased zone of inhibition around the wells (Fig. 4). The inhibition zones were varied in range of 8 mm to 24 mm depending on the strain and tested concentrations of the fabricated CSP-Cr-NCs (Table 1).

3.3. Effect of synthesized CSP-Cr-NCs on the viability of KYSE-150 and Het-1A cells

Fig. 5(a & b) demonstrates the cell viability of formulated CSP-Cr-NCs treated KYSE-150 cells and normal esophageal epithelial Het-1A cells, which was assessed by MTT assay. Our finding evidenced that the CSP-Cr-NCs treatment remarkably suppressed the KYSE-150 cell viability, when compared with control (Fig. 5a). But it did not affected the viability of normal Het-1A cells (Fig. 5b). The increased doses of CSP-Cr-NCs i.e. 0.5–10 µg were effectively decreased the KYSE-

150 cell viability. The IC50 level of CSP-Cr-NCs were noted at 2.5 and 5 µg against KYSE-150 cells and the same dosage did not affected the viability of normal Het-1A cells. Therefore, the 2.5 and 5 µg of CSP-Cr-NCs were selected for the further assays.

3.4. Effect of synthesized CSP-Cr-NCs on the ROS production, MMP level, and apoptotic cell death in the KYSE-150 cells

The effects of CSP-Cr-NCs on the intracellular ROS generation, MMP level, and apoptotic cell death in KYSE-150 cells were assessed by different fluorescence staining techniques and data were displayed in the Fig. 6(a-d). The Fig. 6(a) demonstrates the level of ROS production in the KYSE-150 cells. The 2.5 and 5 µg of synthesized CSP-Cr-NCs administered KYSE-150 cells demonstrated the increased green fluorescence than the control cells, which proved the augmented ROS production. The finding of Rh-123 staining revealed the decreased green fluorescence on the 2.5 and 5 µg treated KYSE-150 cells while, control cells exhibited increased green fluorescence. These finding proved that CSP-Cr-NCs treatment effectively decreased the MMP level in the KYSE-150 cells (Fig. 6b). The outcomes of dual staining and PI staining witnessed that the CSP-Cr-NCs improved the apoptotic cell death in KYSE-150 cells. The 2.5 and 5 µg of CSP-Cr-NCs treated KYSE-150 cells revealed the intense orange/yellow fluorescence than control (Fig. 6c). In PI stain-
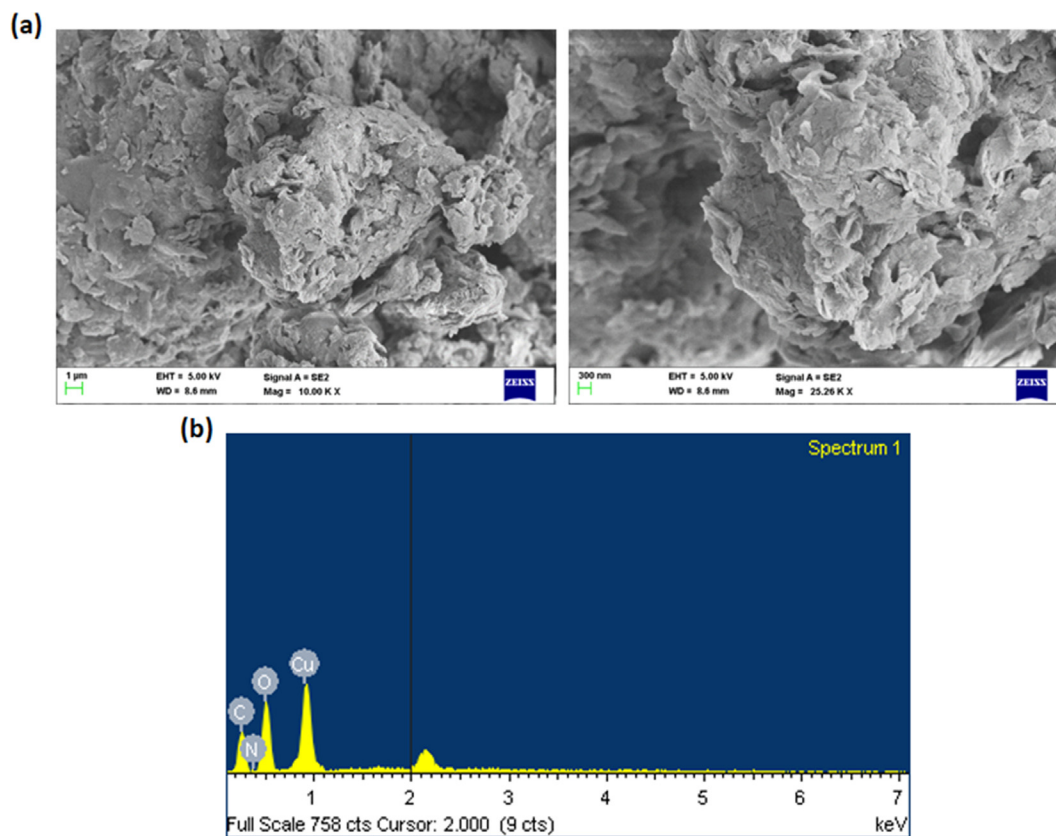
Fig. 3   SEM and EDX analysis of CSP-Cr-NCs. The images of SEM analysis demonstrated the tetragonal and agglomerated morphological appearances **(a)**. The EDX analysis exhibited the occurence of carbon, nitrogen, oxygen, and copper elements in the formulated CSP-Cr-NCs **(b)**.
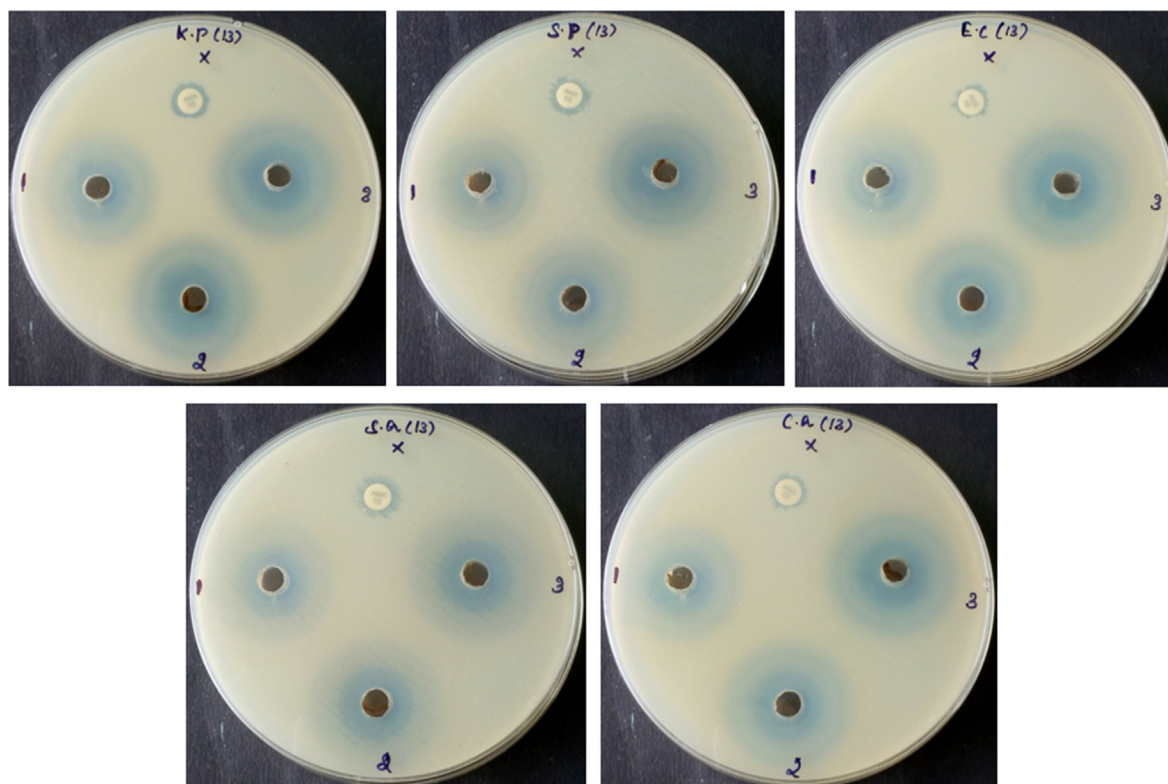
Fig. 4 **Antimicrobial activity of the CSP-Cr-NCs**. Revealed that the formulated CSP-Cr-NCs exhibited the remarkable antimicrobial properoty against the tested pathogens i.e. *S. pneumoniae, K. pneumoniae, E. coli, S. aureus,* and *C. albicans*. The inhibition zones were observed around 8 to 24 mm based on the strain and tested concentration of CSP-Cr-NCs.

Table 1 Antimicrobial activity of the CSP-Cr-NCs.

Species name	40 µl (mm)	50 µl (mm)	60 µl (mm)	Amx (mm)
K. pneumoniae	16	17.5	17	9
S. aureus	17	17.5	18	10.5
E. coli	16	16.5	17	7.5
S. pneumoniae	22	21.5	24	10
C. albicans	15	14.5	16.5	8

The inhibition zones against the tested strains were observed around 8 to 24 mm based on the strain and tested concentration of CSP-Cr-NCs. Data were displayed as mean ± SD of triplicate assays. Results were assessed statistically by one-way ANOVA and Duncan's multiple range assay. '*' indicates $p < 0.05$ compared with control.

ing, the 2.5 and 5 µg of CSP-Cr-NCs administered KYSE-150 cells displayed the increased red fluorescence, while control cells demonstrated slight red fluorescence (Fig. 6d). These findings witnessed evidenced that the CSP-Cr-NCs appreciably enhanced the apoptotic cell death in the KYSE-150 cells.
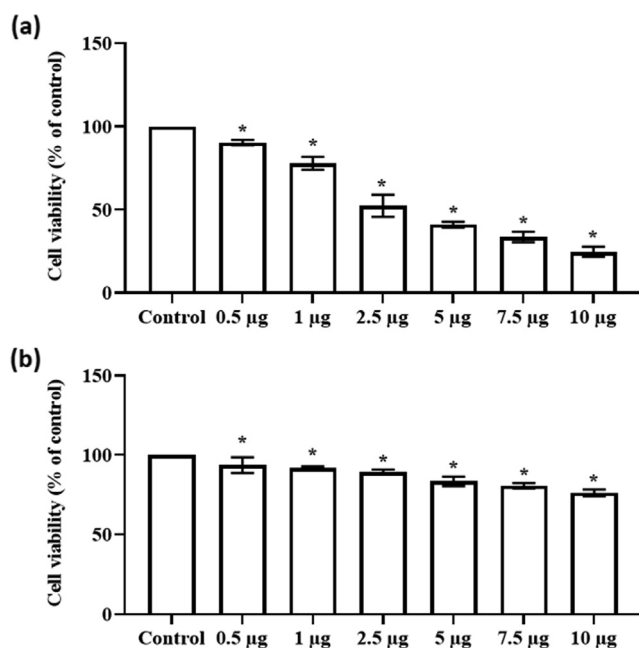
3.5. Effect of synthesized CSP-Cr-NCs treatment on the KYSE-150 cell viability

The effect of CSP-Cr-NCs treatment on the KYSE-150 cell viability were assessed by trypan blue staining method and data were showed in the Fig. 7. The untreated control cells demonstrated less number of stained cells, which proves the higher viable cells. However, the 2.5 and 5 mg/kg of fabricated CSP-Cr-NCs administered KYSE-150 cells exhibited increased number of stained cells that witnessed the elevated cell death due to the CSP-Cr-NCs treatment (Fig. 7).

3.6. Effect of CSP-Cr-NCs treatment on the cell migration of KYSE-150 cells

The wound scratch assay was performed to examine the inhibitory role of CSP-Cr-NCs on the migration of KYSE-150 cells. After 24 h period, the untreated control cells showed increased wound closure, which proved the improved migration of KYSE-150 cells. Interestingly, the treatment with 2.5 and 5 µg of CSP-Cr-NCs treated KYSE-150 cells demonstrated less wound closure, which proved the decreased cell migration (Fig. 8). The findings witnessed that the CSP-Cr-NCs treatment effectively inhibited the migration of KYSE-150 cells.

Fig. 5   Effect of synthesized CSP-Cr-NCs on the viability of KYSE-150 and Het-1A cells. The treatment with formulated CSP-Cr-NCs at different doses such as 0.5–10 μg effectively inhibited the KYSE-150 cell growth **(a)**. The same dose of CSP-Cr-NCs did not affected the viability of normal Het-1A cells **(b)**. The IC50 dose was observed at 2.5 μg against KYSE-150 cells. Data were displayed as mean ± SD of triplicate assays. Results were evaluated statistically by one-way ANOVA and Duncan's multiple range assay. '*' indicates p < 0.05 compared with control.

3.7. Effect of CSP-Cr-NCs treatment on the levels of oxidant and antioxidant biomarkers in the KYSE-150 cells

Fig. 9 exhibits the effect of CSP-Cr-NCs on the oxidant and antioxidant status in the KYSE-150 cells. The content of TBARS was drastically improved in the KYSE-150 cells treated with 2.5 and 5 μg of CSP-Cr-NCs than the untreated control cells. Additionally, the level of GSH and SOD activity was found decreased in the CSP-Cr-NCs supplemented KYSE-150 cells than then control. This finding confirmed that CSP-Cr-NCs treatment aggravates the oxidative stress in the KYSE-150 cells (Fig. 9).

4. Discussion

Esophageal cancer is one of the sixth leading causes of cancer-related mortalities with increased prevalence in each year worldwide. Esophageal cancer is usually detected at later stage and it has the poor prognosis with 10% of 5-year survival rate. The tumor eradication surgery followed by the chemo and radiotherapy are the conventional approaches for the cancer treatment (Liyanage et al., 2019). The combined administration of 5-Fluorouracil and cisplatin are the general treatment approach for esophageal cancer (Baba et al., 2014). Though, the outcomes are often unsatisfactory because of the drug resistance (Yu et al., 2015). At present, esophagectomy is a main approach to treat the esophageal cancer (Takeuchi et al., 2014). Due to the considerable morbidity, toxicity, and

poor response of currently used therapies, the need for the exploration of novel strategies to overcome these issues are highly warranted. A previous study reported that the formation of nanoscale drug delivery system, can make sure the accurate cancer targeting ability with lesser adverse effects (Huang et al., 2019). The nanomaterials can be easily penetrate the cell barriers because of its biological nature (Chaturvedi et al., 2019).

Over the decades, nanomaterials were utilized in the cancer treatments, because of its passive and active targeting. Additionally, several drugs can be utilized to treat cancers but the sensitivity of these drugs can result in several adverse effects and damage to the normal cells. For that reason, manifold researches has focused on various nanomaterials with the combination of anticancer drugs in order to achieve the safe and effective anticancer formulation with lesser side effects (Ye et al., 2018). Nanomedicines have been broadly examined for the cancer-targeted drug delivery and decreasing adverse of chemotherapeutic agents (Peer et al., 2007). Chitosan is a well known biopolymer and effective carrier for nano-drugs with increased pharmacological and bio-medical benefits due to its several striking character like safety, low cost, biocompatibility and degradability (Zhang and Wang, 2013). In this work, we evidenced that the fabricated CSP-Cr-NCs demonstrated the remarkable *in vitro* anticancer activity against the esophageal cancer KYSE-150 cells via augmenting the apoptotic cell death. Furthermore, the formulated CSP-Cr-NCs also exhibited the remarkable antimicrobial properties. Our current results were coincides with the previous report by Ali-Gethami and Al-Qasmi (2021).

A slight increase in intracellular ROS level may lead to the stimulation of oncogenes, which are participated in cell proliferation, mitochondrial and angiogenesis dysfunction, thus facilitates to the signaling molecule in tumor survival (Kumari et al., 2018). Conversely, when the ROS level was further increased, they can overwhelm the antioxidant defence mechanisms, leading to cell death (Galadari et al., 2017). The ROS is needed to regulate the normal biological functions, and a marked reduction or increase in ROS level can result in cytotoxicity in tumor cells (Raza et al., 2017; DeBerardinis and Chandel, 2016). Though increased ROS production is tightly connected with the mitochondrial dysfunction. Additionally, the abnormal ROS accumulation causes oxidative stress and damages of DNA (Redza-Dutordoir and Averill-Bates, 2016; Orrenius et al., 2015). The triggering of increased ROS generation in tumor cells is a general mechanism of most non-surgical therapies like radio and chemotherapies (Sun et al., 2013). Stimulating ROS accumulation is reported as a hopeful strategy in cancer treatment (Watson, 2013). Here, our findings demonstrated that the CSP-Cr-NCs improved the ROS accumulation in KYSE-150 cells. This finding proved that the CSP-Cr-NCs administration could facilitate to the ROS-mediated cell death in KYSE-150 cells.

Additionally, tumor cells has hypermetabolism that generates huge quantity of ROS than in normal cells. On the other hand, tumor cells have remarkable antioxidant potential that facilitate sustaining the redox equilibrium (Prasad et al., 2017). The augmented ROS interrupts redox balance and trigger injury to the tumor cells and result in cell death. Our finding from this study evidenced that the CSP-Cr-NCs treatment improved the TBARS status and reduced the GSH content and SOD activity in the KYSE-150 cells. This finding proved
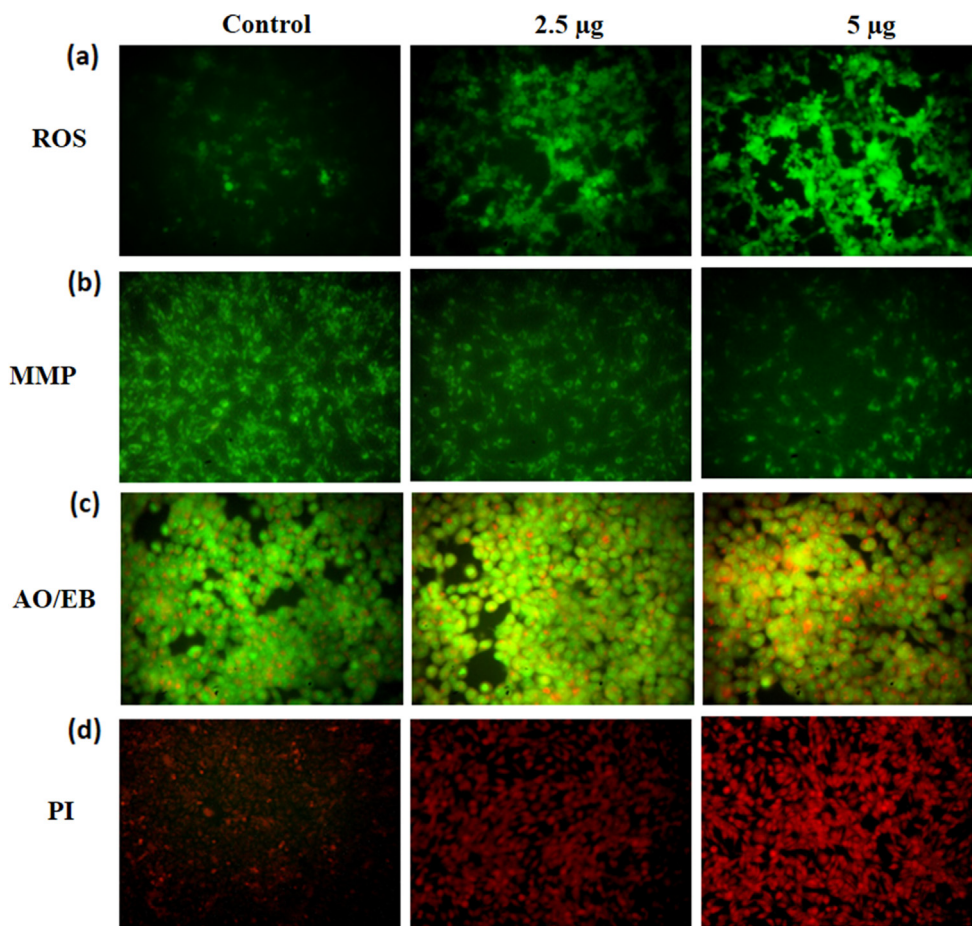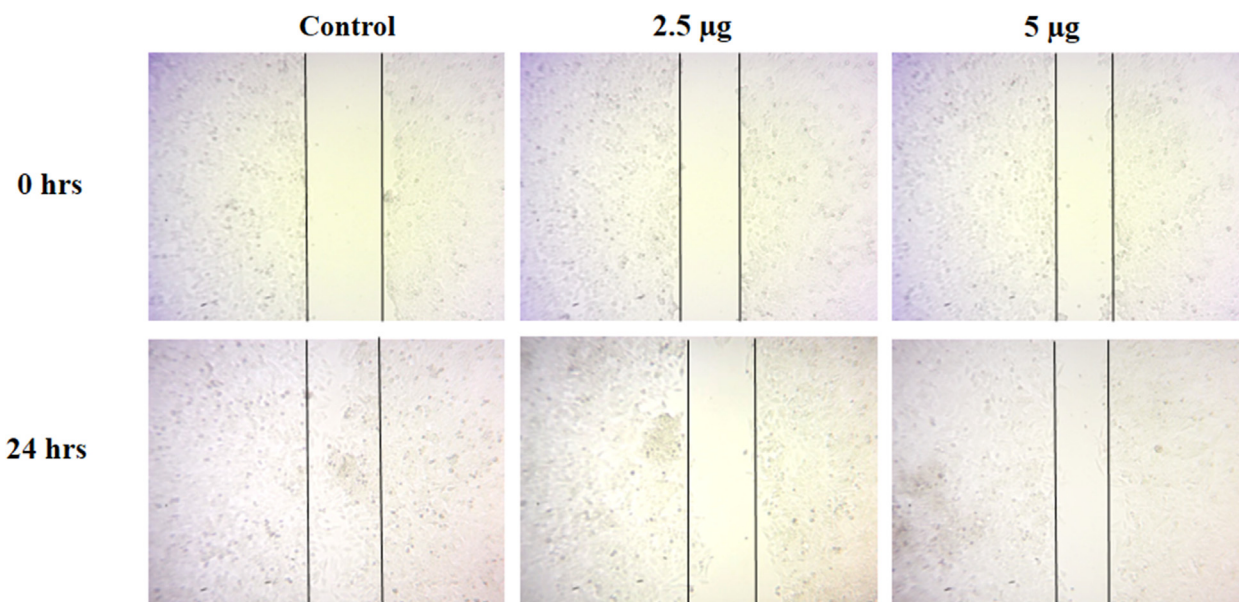
Fig. 6   Effect of synthesized CSP-Cr-NCs on the ROS production, MMP level, and apoptosis in the KYSE-150 cells. The increased green fluorescence was noted on the 2.5 and 5 μg of CSP-Cr-NCs treated KYSE-150 cells than control that proves the higher ROS generation **(a)**. The 2.5 and 5 μg of CSP-Cr-NCs administered KYSE-150 cells exhibited the depleted green fluorescence than control cells that suggest the reduced MMP level **(b)**. The 2.5 and 5 μg of formulated CSP-Cr-NCs treated KYSE-150 cells revealed a higher yellow/orange fluorescence than control that proves the apoptotic cell deaths **(c)**. The KYSE-150 cells supplemented with 2.5 and 5 μg of formulated CSP-Cr-NCs exhibited the increased red fluorescence than control, which evidenced the elevated apoptotic cell death **(d)**.
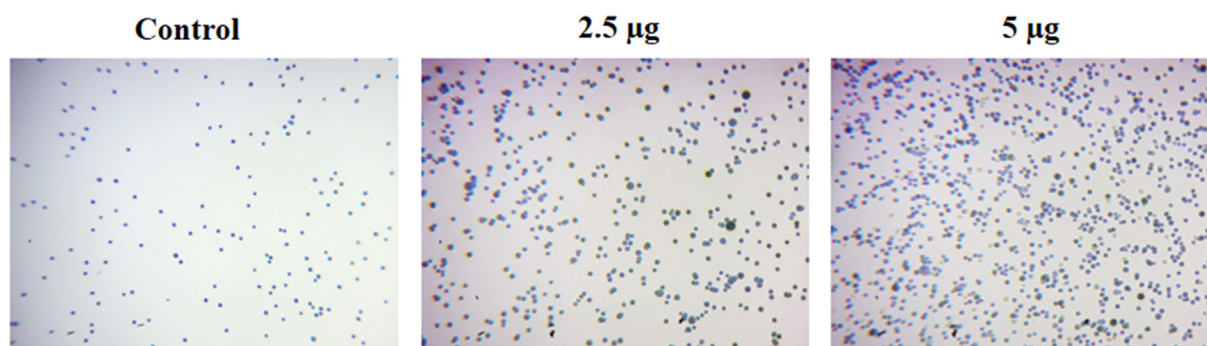

Fig. 7   Effect of synthesized CSP-Cr-NCs treatment on the KYSE-150 cell viability. The treatment with the 2.5 and 5 μg of formulated CSP-Cr-NCs demonstrated the augmented trypan blue stained cells than control, which confirms the higher cell death.

that the CSP-Cr-NCs treatment could worsen the oxidative stress and facilitates to cell death in KYSE-150 cells. Previously, Zhang et al. (2021) already highlighted that the crocin effectively increase the lipid peroxidation and decrease the SOD, CAT, and GSH in the thyroid cancer FTC-133 cells. Our present findings were supported by this earlier report.

The resistance to chemotherapy and tumor metastasis often lead to poor prognosis (Wang et al., 2017). The induction of apoptosis in tumor cells is a key approach for cancer treatment. The anticancer drugs with successful apoptosis-triggering ability result in tumor cell necrosis by increasing pro-apoptotic signaling (Cotter, 2009). The dysregulation of

Fig. 8   Effect of CSP-Cr-NCs treatment on the cell migration of KYSE-150 cells. The KYSE-150 cells administered with 2.5 and 5 μg of synthesized CSP-Cr-NCs demonstrated reduced wound closure rate, while untreated control cells showed increased wound closure level, suggest that CSP-Cr-NCs treatment inhibited the migration of KYSE-150 cells.
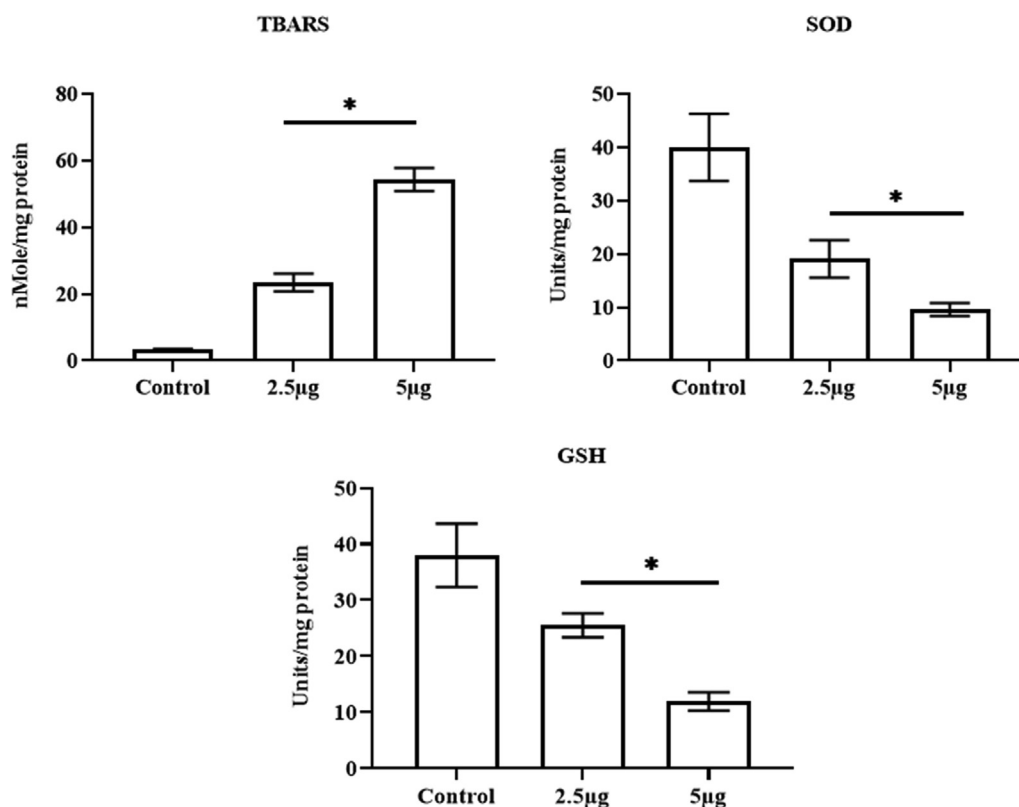
Fig. 9   Effect of CSP-Cr-NCs treatment on the levels of oxidant and antioxidant biomarkers in the KYSE-150 cells. The 2.5 and 5 μg of fabricated CSP-Cr-NCs treated KYSE-150 cells revealed a augmented TBARS level, depleted GSH content and SOD activity than control. Data were displayed as mean ± SD of triplicate assays. Results were evaluated statistically by one-way ANOVA and Duncan's multiple range assay. '*' indicates $p < 0.05$ compared with control.

apoptotic events has straight connection with several ailments, including cancer development (Letai, 2017). The flaws in apoptosis can improve cancer growth, and also make tumor cells resistant to therapies. Hence, the apoptosis evasion is a remarkable event of cancer growth (Hassan et al., 2014). The tumor cells demonstrate impaired apoptotic pathway that

facilitates to the tumor metastasis and development (Plati et al., 2008). Additionally, the main target of cancer treatment is to induce the apoptosis in tumor cells (Carneiro and El-Deiry, 2020). In this work, we witnessed that the CSP-Cr-NCs increased the apoptosis in KYSE-150 cells. Additionally, the mitochondria plays imperative role in tumor cell necrosis though the depolarization of membrane potential (Kalainayakan et al. 2018). The mitochondria of normal and tumor cells has several variations due to the deregulated ROS metabolism in tumor cells (Wang et al., 2017). We also noticed that the formulated CSP-Cr-NCs remarkably decreased the MMP status in the KYSE-150 cells.

The increased ROS production in tumor cells, which over-whelm the antioxidant defense mechanisms were highlighted to trigger apoptosis through several downstream cascades (Zhou et al., 2019). ROS plays a major role in triggering apoptosis under pathological and physiological circumstances (D'Autreaux and Toledano, 2007; Liu et al., 2008). ROS are well known to stimulate the apoptosis in cells (Langer et al., 2008). The numerous anticancer candidates like trisenox (Jeanne et al., 2010), paclitaxel (Alexandre et al., 2007), and 2-methoxyestradiol (Gao et al., 2005) was reported to improve the ROS accumulation in tumor cells. These findings suggest that drugs, which can regulate cellular oxidative and redox signaling in tumor cells could provide opportunities for cancer treatment. Similarly, our outcomes evidenced that the CSP-Cr-NCs remarkably increased the ROS production, aggravates oxidative stress and antioxidants balance, and improved the apoptosis in the KYSE-150 cells.

5. Conclusion

Taken together, our findings confirmed that the formulated CSP-Cr-NCs treatment showed effective *in vitro* anticancer activity against eso-phageal cancer KYSE-150 cells. The CSP-Cr-NCs treatment increased the ROS accumulation, decreased MMP, aggravates oxidative stress, and stimulated the apoptosis in the KYSE-150 cells. Furthermore, the CSP-Cr-NCs also demonstrated the effective antimicrobial proper-ties. Hence, it was clear that the CSP-Cr-NCs were effective against esophageal cancer and it could be a anticancer nano-formulation in the future to treat the esophageal cancer.

Declaration of Competing Interest

The authors declare that they have no known competing financial interests or personal relationships that could have appeared to influence the work reported in this paper.

Acknowledgement

References

Afzal, M., Uzzafar, A., Alharbi, K.S., Alruwaili, N.K., Al-Abassi, F. A., Al-Malki, A.A.L., Kazmi, I., Kumar, V., Kamal, M.A., Nadeem, M.S., Aslam, M., Anwar, F., 2021. Nanomedicine in treatment of breast cancer—A challenge to conventional therapy. Semin. Cancer Biol. 69, 279–292.

Alavizadeh, S.H., Hosseinzadeh, H., 2014. Bioactivity assessment and toxicity of crocin: a comprehensive review. Food Chem. Toxicol. 64, 65–80.

Alexandre, J., Hu, Y., Lu, W., Pelicano, H., Huang, P., 2007. Novel action of paclitaxel against cancer cells: bystander effect mediated by reactive oxygen species. Cancer Res. 67, 3512–3517.

Ali-Gethami, W., Al-Qasmi, N., 2021. Antimicrobial activity of Ca-alginate/chitosan nanocomposite loaded with camptothecin. Poly-mers (Basel) 13 (20), 3559.

Amerizadeh, F., Rezaei, N., Rahmani, F., Hassanian, S.M., Moradi-Marjaneh, R., Fiuji, H., Boroumand, N., Nosrati-Tirkani, A., Ghayour-Mobarhan, M., Ferns, G.A., Khazaei, M., Avan, A., 2018. Crocin synergistically enhances the antiproliferative activity of 5-flurouracil through Wnt/PI3K pathway in a mouse model of colitis-associated colorectal cancer. J. Cell. Biochem. 119, 10250–10261.

Baba, Y., Watanabe, M., Yoshida, N., Baba, H., 2014. Neoadjuvant treatment for esophageal squamous cell carcinoma. World J. Gastrointestinal Oncol. 6, 121–128.

Bor, G., Mat Azmi, I.D., Yaghmur, A., 2019. Nanomedicines for cancer therapy: current status, challenges and future prospects. Ther. Deliv. 10, 113–132.

Bray, F., Ferlay, J., Soerjomataram, I., Siegel, R.L., Torre, L.A., Jemal, A., 2018. Global cancer statistics 2018: GLOBOCAN estimates of incidence and mortality worldwide for 36 cancers in 185 countries. CA. Cancer J. Clin. 68, 394–424.

Carneiro, B.A., El-Deiry, W.S., 2020. Targeting apoptosis in cancer therapy. Nat. Rev. Clin. Oncol. 17, 395–417.

Chadchawan, S., Pichyangkura, R., 2015. Biostimulant activity of chitosan in horticulture. Sci. Horticulturae. 196, 49–65.

Chaturvedi, V.K., Singh, A., Singh, V.K., Singh, M.P., 2019. Cancer nanotechnology: a new revolution for cancer diagnosis and therapy. Curr. Drug Metab. 20, 416–429.

Cheng, L., Yan, B., Chen, K., Jiang, Z., Zhou, C., Cao, J., Qian, W., Li, J., Sun, L., Ma, J., Ma, Q., Sha, H., 2018. Resveratrol-induced downregulation of NAF-1 enhances the sensitivity of pancreatic cancer cells to gemcitabine via the ROS/Nrf2 signaling pathways. Oxid. Med. Cell. Longev. 2018, 9482018.

Cotter, T.G., 2009. Apoptosis and cancer: the genesis of a research field. Nat. Rev. Cancer 9, 501–507.

D'Autreaux, B., Toledano, M.B., 2007. ROS as signalling molecules: mechanisms that generate specificity in ROS homeostasis. Nat. Rev. Mol. Cell Biol. 8, 813–824.

DeBerardinis, R.J., Chandel, N.S., 2016. Fundamentals of cancer metabolism. Sci. Adv. 2, e1600200.

Deng, L.Y., Li, J.C., Lu, S.Y., Su, Y., 2019. Crocin inhibits proliferation and induces apoptosis through suppressing MYCN expression in retinoblastoma. J. Biochem. Mol. Toxicol. 33, e22292.

El-Say, K.M., El-Sawy, H.S., 2017. Polymeric nanoparticles: Promis-ing platform for drug delivery. Int. J. Pharm. 528, 675–691.

Galadari, S., Rahman, A., Pallichankandy, S., Thayyullathil, F., 2017. Reactive oxygen species and cancer paradox: to promote or to suppress? Free Radic. Biol. Med. 104, 144–164.

Gao, N., Rahmani, M., Dent, P., Grant, S., 2005. 2-Methoxyestradiol-induced apoptosis in human leukemia cells proceeds through a reactive oxygen species and Akt-dependent process. Oncogene 24, 3797–3809.

Hadjesfandiari, N., Parambath, A., 2018. 13—stealth coatings for nanoparticles: polyethylene glycol alternatives. Woodhead Pub-lishing, Sawston, pp. 345–361.

Hassan, M., Watari, H., AbuAlmaaty, A., Ohba, Y., Sakuragi, N., 2014. Apoptosis and molecular targeting therapy in cancer. Biomed Res. Int. 2014, 150845.

Hosseinzadeh, H., Abootorabi, A., Sadeghnia, H.R., 2008. Protective effect of Crocus sativus Stigma extract and crocin (trans-crocin 4) on methyl methanesulfonate-induced DNA damage in mice organs. DNA Cell Biol. 27, 657–664.

Huang, D., Wu, K., Zhang, Y., Ni, Z., Zhu, X., Zhu, C., 2019. Recent Advances in Tissue plasminogen activator-based nanothrombolysis for ischemic stroke. 58: 159.

Huang, L., Huang, J., Huang, J., Xue, H., Liang, Z., Wu, J., Chen, C., 2020. Nanomedicine—A promising therapy for hematological malignancies. Biomater. Sci., 1–34

Hugtenburg, J.G., Timmers, L., Beckeringh, J.J., 2019. Pharmaceutical care for cancer outpatients. In: Alves da Costa, F., van Mil, J., Alvarez-Risco, A. (Eds.), The Pharmacist Guide to Implementing Pharmaceutical Care, Springer, Cham, pp. 397–419.

Jeanne, M., Lallemand-Breitenbach, V., Ferhi, O., Koken, M., Le Bras, M., Duffort, S., Peres, L., Berthier, C., Soilihi, H., Raught, B., de The, H., 2010. PML/RARA oxidation and arsenic binding initiate the antileukemia response of As2O3. Cancer Cell 18, 88–98.

Kalainayakan, S.P., FitzGerald, K.E., Konduri, P.C., Vidal, C., Zhang, L., 2018. Essential roles of mitochondrial and heme function in lung cancer bioenergetics and tumorigenesis. Cell Biosci. 8 (1), 56.

Kim, S.J., Kim, H.S., Seo, Y.R., 2019. Understanding of ROS-inducing strategy in anticancer therapy. Oxid. Med. Cell. Longev. 2019, 5381692.

Kumari, S., Badana, A.K., Malla, R., 2018. Reactive Oxygen Species: A Key Constituent in Cancer Survival. Biomark. Insights, 13, 1177271918755391.

Kuo, K.T., Chen, C.L., Chou, T.Y., Yeh, C.T., Lee, W.H., Wang, L. S., 2016. Nm23H1 mediates tumor invasion in esophageal squamous cell carcinoma by regulation of CLDN1 through the AKT signaling. Oncogenesis 5, e239.

Langer, D.A., Das, A., Semela, D., Kang-Decker, N., Hendrickson, H., Bronk, S.F., Katusic, Z.S., Gores, G.J., Shah, V.H., 2008. Nitric oxide promotes caspase-independent hepatic stellate cell apoptosis through the generation of reactive oxygen species. Hepatology 47, 1983–1993.

Letai, A., 2017. Apoptosis and cancer. Annu. Rev. Cancer Biol. 1, 275–294.

Liu, B., St, C.Y., Clair, D.K., 2008. ROS and p53: a versatile partnership. Free Radic. Biol. Med. 44, 1529–1535.

Liyanage, P.Y., Hettiarachchi, S.D., Zhou, Y., Ouhtit, A., Seven, E.S., Oztan, C.Y., Celik, E., Leblanc, R.M., 2019. Nanoparticle-mediated targeted drug delivery for breast cancer treatment. Biochim. Biophys. Acta, Rev. Cancer 1871, 419–433.

Mishra, P., Nayak, B., Dey, R.K., 2016. PEGylation in anti-cancer therapy: an overview. Asian J. Pharm. Sci. 11, 337–348.

Mollaei, H., Safaralizadeh, R., Babaei, E., Abedini, M.R., Hoshyar, R., 2017. The anti-proliferative and apoptotic effects of crocin on chemosensitive and chemoresistant cervical cancer cells. Biomed. Pharmacother. 94, 307–316.

Munawar, A., Mohammed, J.T., Syeda, M., Wasan, K.M., Wasan, E. K., 2017. An overview of chitosan nanoparticles and its application in non-parenteral drug delivery. Pharmaceutics 9, 53.

O'Sullivan, K.E., Michielsen, A.J., O'Regan, E., Cathcart, M.C., Moore, G., Breen, E., Segurado, R., Reynolds, J.V., Lysaght, J., O'Sullivan, J., 2018. pSTAT3 levels have divergent expression patterns and associations with survival in squamous cell carcinoma and adenocarcinoma of the oesophagus. Int. J. Mol. Sci. 19, 15.

Orrenius, S., Gogvadze, V., Zhivotovsky, B., 2015. Calcium and mitochondria in the regulation of cell death. Biochem. Biophys. Res. Commun. 460, 72–81.

Peer, D., Karp, J.M., Hong, S., Farokhzad, O.C., Margalit, R., Langer, R., 2007. Nanocarriers as an emerging platform for cancer therapy. Nat. Nanotechnol. 2, 751–760.

Plati, J., Bucur, O., Khosravi-Far, R., 2008. Dysregulation of apoptotic signaling in cancer: Molecular mechanisms and therapeutic opportunities. J. Cell. Biochem. 104, 1124–1149.

Prasad, S., Gupta, S.C., Tyagi, A.K., 2017. Reactive oxygen species (ROS) and cancer: Role of antioxidative nutraceuticals. Cancer Lett. 387, 95–105.

Qi, L., Xu, Z., Jiang, X., Hu, C., Zou, X., 2004. Preparation and antibacterial activity of chitosan nanoparticles. Carbohyd. Res. 339, 2693–2700.

Raza, M.H., Siraj, S., Arshad, A., Waheed, U., Aldakheel, F., Alduraywish, S., Arshad, M., 2017. ROS-modulated therapeutic approaches in cancer treatment. J. Cancer Res. Clin. Oncol. 143 (9), 1789–1809.

Redza-Dutordoir, M., Averill-Bates, D.A., 2016. Activation of apoptosis signalling pathways by reactive oxygen species. BBA 1863, 2977–2992.

Suk, J.S., Xu, Q., Kim, N., Hanes, J., Ensign, L.M., 2016. PEGylation as a strategy for improving nanoparticle-based drug and gene delivery. Adv. Drug Deliv. Rev. 99, 28–51.

Sun, X., Ai, M., Wang, Y., Shen, S., Gu, Y., Jin, Y., Zhou, Z., Long, Y., Yu, Q., 2013. Selective induction of tumor cell apoptosis by a novel P450-mediated reactive oxygen species (ROS) inducer methyl 3-(4-nitrophenyl) propiolate. J. Biol. Chem. 288, 8826–8837.

Swain, S., Sahu, P.K., Babu, S.M., 2016. Nanoparticles for cancer targeting: current and future directions. Curr. Drug Deliv. 13 (8), 1290–1302.

Takeuchi, H., Miyata, H., Gotoh, M., Kitagawa, Y., Baba, H., Kimura, W., Tomita, N., Nakagoe, T., Shimada, M., Sugihara, K., Mori, M., 2014. A risk model for esophagectomy using data of 5354 patients included in a Japanese nationwide web-based database. Ann. Surg. 260, 259–266.

Wang, J.P., Hsieh, C.H., Liu, C.Y., Lin, K.H., Wu, P.T., Chen, K.M., Fang, K., 2017a. Reactive oxygen species-driven mitochondrial injury induces apoptosis by teroxirone in human non-small cell lung cancer cells. Oncol. Lett. 14 (3), 3503–3509.

Wang, Y., Li, Y.J., Huang, Y.H., Zheng, C.C., Yin, X.F., Li, B., He, Q.Y., 2018. Liensinine perchlorate inhibits colorectal cancer tumorigenesis by inducing mitochondrial dysfunction and apoptosis. Food Funct. 9, 5536–5546.

Wang, S., Huang, S., Sun, Y.L., 2017b. Epithelial-mesenchymal transition in pancreatic cancer: a review. Biomed. Res. Int. 2017, 2646148.

Wathoni, N., Rusdin, A., Febriani, E., Purnama, D., Daulay, W., Azhary, S.Y., Panatarani, C., Joni, I.M., Lesmana, R., Motoyama, K., Muchtaridi, M., 2019. Formulation and Characterization of α-Mangostin in Chitosan Nanoparticles Coated by Sodium Alginate, Sodium Silicate, and Polyethylene Glycol. J. Pharm. Bioallied Sci. 11 (4), S619–S627.

Watson, J., 2013. Oxidants, antioxidants and the current incurability of metastatic cancers. Open Biol. 3, 120144.

Wilkosz, N., Łazarski, G., Kovacik, L., Gargas, P., Nowakowska, M., Jamróz, D., Kepczynski, M., 2018. Molecular insight into drug-loading capacity of PEG–PLGA nanoparticles for itraconazole. J. Phys. Chem. B 122, 7080–7090.

Yang, H., Villani, R.M., Wang, H., Simpson, M.J., Roberts, M.S., Tang, M., Liang, X., 2018. The role of cellular reactive oxygen species in cancer chemotherapy. J. Exp. Clin. Cancer Res. 37, 266.

Yaribeygi, H., Mohammadi, M.T., Sahebkar, A., 2018. Crocin potentiates antioxidant defense system and improves oxidative damage in liver tissue in diabetic rats. Biomed. Pharmacother. 98, 333–337.

Ye, F., Zhao, Y., El-Sayed, R., Muhammed, M., Hassan, M.J.N.T., 2018. Advances in nanotechnology for cancer biomarkers. 18, 103-23.

Yu, P., Cheng, X., Du, Y., Yang, L., Huang, L., 2015. Significance of MDR-related proteins in the postoperative individualized chemotherapy of gastric cancer. J. Cancer Res. Ther. 11, 46–50.

Zhang, X.Y., Wang, L.X.J., 2013. Effects of surface modification on the properties of magnetic nanoparticles/PLA composite drug carriers and in vitro controlled release study. Colloid Surf. A-Physicochem. Eng. 2013 (431), 80–86.

Zhang, Y., Zhu, M., Mohan, S.K., Hao, Z., 2021 Jan. Crocin treatment promotes the oxidative stress and apoptosis in human

thyroid cancer cells FTC-133 through the inhibition of STAT/JAK signaling pathway. J. Biochem. Mol. Toxicol. 35, (1) e22608.

Zhou, J., Zhang, L., Wang, M., Zhou, L., Feng, X., Yu, L., Lan, J., Gao, W., Zhang, C., Bu, Y., Huang, C., Zhang, H., Lei, Y., 2019a. CPX Targeting DJ-1 triggers ROS-induced cell death and protective autophagy in colorectal cancer. Theranostics 9, 5577–5594.

Zhou, Y., Xu, Q.H., Shang, J.J., Lu, L.H., Chen, G.Y., 2019b. Crocin inhibits the migration, invasion, and epithelial-mesenchymal transitionof gastric cancer cells via miR-320/KLF5/HIF-1α signaling. J. Cell. Physiol. 234, 17876–17885.

Zhu, K., Yang, C., Dai, H., Li, J., Liu, W., Luo, Y., Zhang, X., Wang, Q., 2019. Crocin inhibits titanium particle-induced inflammation and promotes osteogenesis by regulating macrophage polarization. Int. Immunopharmacol. 76, 105865.

Zhu, H., Sarkar, S., Scott, L., Danelisen, I., Trush, M.A., Jia, Z., Li, Y.R., 2016. Doxorubicin redox biology: redox cycling, topoisomerase inhibition, and oxidative stress. React. Oxyg. Species 1, 189–198.